scientific reports



OPEN The dominant synoptic patterns and basic characteristics of regional snowstorms in Northern Xinjiang over the past 70 years

Chunyang Li¹, Abuduwaili Abulikemu¹⊠, Xin Xu², Shushi Zhang³,⁴, Zhiyi Li¹, Mingjie Ma¹, Abidan Abuduaini¹ & Zulipina Kadier¹

This study employs the PCT objective classification method to analyze 134 regional snowstorm events in northern Xinjiang (NX) during 1953-2022 using observational and reanalysis data, identifying four primary synoptic types that are all associated with polar vortex activity. This study investigated the snowstorm characteristics associated with the synoptic patterns, along with the features of upper- and lower-level jet streams and moisture transport. The results show that 66.4% of cases are related to eccentric polar vortex patterns while 33.6% are connected to dipole vortices, with each synoptic type exhibiting distinct formation mechanisms. The research demonstrates that variations in upper- and lower-level jets directly influence snowstorm frequency and spatial distribution, while also affecting moisture transport characteristics. Moisture is primarily transported into the region through western boundaries and out through eastern boundaries, with significant additional input from northern boundaries, patterns that are fundamentally determined by differences in large-scale circulation systems. These findings provide important insights into the atmospheric dynamics governing snowstorm formation in NX.

Keyword Regional snowstorm, Moisture transport, Northern Xinjiang, Classification

Snowstorms have always been a key focus and challenge in meteorological forecasting during winter for northern Xinjiang (NX), resulting in significant disasters across various sectors, including transportation, infrastructure, agriculture, and animal husbandry. At the same time, snowstorms are one of the most severe natural disasters in mid-high latitudes in the northern hemisphere during winter, causing significant damage to the economy and human lives¹⁻³. Extreme weather and climate events have become more severe and more frequent⁴⁻⁷, along with the backdrop of global warming. Against this backdrop, the number of snowstorm events in NX has also increased8. Gaining a deeper understanding of the spatiotemporal distribution, causes, and typical synoptic patterns of snowstorm events is essential for improving snowstorm forecasting accuracy.

The occurrence and development mechanisms of snowstorms are quite complex, and many previous studies investigated the formation mechanisms, development features, and influencing factors of snowstorms to gain a deeper understanding of them⁹⁻¹¹. It typically combines observational data, reanalysis data, and numerical simulations to investigate the circulation backgrounds of snowstorm occurrence¹², moisture transport features¹³, and some effects of multiple factors, including topography^{14–16}, and water body^{17,18}. Recently, more and more methods have been used to carry out relevant research, including observation means such as dual-polarization radar and microwave radiometers¹⁹, multiple microphysical schemes and data assimilation along with various data sources in numerical simulation, and deep (machine) learning^{20,21}.

Large-sample statistical studies help improve the understanding of extreme weather events^{22,23}. In particular, they are useful for revealing synoptic patterns and regional characteristics. These studies can summarize the frequency, intensity, spatial variability, and relationships between extreme synoptic events and atmospheric circulation patterns^{24,25}. One approach is to identify typical synoptic types, which allows for determining the

¹Xinjiang Key Laboratory of Oasis Ecology, College of Geography and Remote Sensing Sciences, Xinjiang University, Urumqi, China. ²Key Laboratory of Mesoscale Severe Weather (Ministry of Education), School of Atmospheric Sciences, Nanjing University, Nanjing, China. ³Nanjing Innovation Institute for Atmospheric Sciences, Chinese Academy of Meteorological Sciences-Jiangsu Meteorological Service, Nanjing, China. ⁴Jiangsu Key Laboratory of Severe Storm Disaster Risk / Key Laboratory of Transportation Meteorology of CMA, Nanjing, China. □email: abduwaly@xju.edu.cn

contributions of different synoptic patterns to extreme events and quantifying the moisture sources and affected regions associated with each type^{26,27}. Through objective classification, it was found that 51.85% of hail days are associated with two main circulation types related to the northern cold frontal system²⁸. Wang et al.²⁹ classified the warm-season rainstorm processes along the southern coast of China and discovered that heavy precipitation mainly occurs under three typical strong low-level onshore winds synoptic patterns. Zeng et al.³⁰ classified hourly extreme precipitation events and found that they are primarily influenced by the Meiyu front and typhoons, with the Meiyu front type further subdivided into two sub-categories. Research on winter snowstorms in NX is relatively limited, making it more urgent to apply new methods for evaluation and analysis.

In studies of snowstorms in NX, subjective classification methods are commonly employed. Yang et al. studied the frequency and spatial distribution of winter snowstorms in NX, and through composite analysis, found that the synoptic patterns influencing snowstorms are related to frontal zones and vortices. Li et al. summarized three typical synoptic types for snowstorms in Urumqi, with the 300 hPa jet and 700 hPa northerly jet being the primary influencing systems, while a northwesterly flow exists at 850 hPa. Wei et al. conducted a subjective classification of snowstorms in Tacheng and found that different types of snowstorms have distinct moisture sources and transport patterns, and are associated with troughs and jets. Additionally, by analyzing the snowfall regions, four types of snowstorms in NX were classified, revealing different moisture transport channels and distinct characteristics of geopotential height anomalies 1. In contrast, objective classification avoids human biases and provides more consistent and scientifically rigorous classification results 28,34. Therefore, conducting objective classification studies of large-scale circulation patterns associated with snowstorms in NX is of great significance for improving snowstorm forecasting and understanding the mechanisms behind their formation.

Compared to previous studies, this paper will conduct a statistical analysis of 70 years of snowstorm events in NX using an objective classification method. This will help to understand the synoptic patterns associated with snowstorm events, obtain the large-scale circulation structures at different levels, and more precisely reveal the climatic background and atmospheric circulation patterns of snowstorm events. This paper mainly addresses two questions: (1) What are the typical synoptic patterns that control snowstorm events in NX during winter? (2) What are the basic characteristics of each synoptic pattern?

Data and methods Data

This study used the 24-h observational precipitation data set from 20:00 to 20:00 of the following day, observed at 50 meteorological stations in NX from 1953 to 2022, provided by the National Meteorological Center of the China Meteorological Administration (CMA), for the selection of snowstorm events, all data are referenced to Coordinated Universal Time (UTC). Besides, the ERA5 reanalysis data (with horizontal resolution of $0.25^{\circ} \times 0.25^{\circ}$ and temporal resolution of 1 h, and the dataset provides global coverage) from 1953 to 2022 provided the European Centre for Medium-Range Weather Forecasts (ECMWF) (https://www.ecmwf.int/en/forecasts /datasets/browse-reanalysis-datasets) was also utilized (the physical quantities employed include wind fields, temperature, geopotential height, specific humidity, and relative humidity, the analysis employed geopotential height data at 500, 700, and 850 hPa levels). Since Xinjiang is an arid and semi-arid region, according to the precipitation intensity standard of Xinjiang³⁵, snowstorms are defined as a precipitation amount of ≥ 12.1 mm within 24 h (the precipitation amount mentioned in this study indicates snow water equivalent value). The definition of regional snowstorms is as follows³⁶: if at least three meteorological stations report snowstorms within 24 h or at least five meteorological stations report snowstorms within 48 h surrounding a snowstorm event, then it is considered a regional snowstorm. This study identified 134 regional snowstorm events using daily observational data from meteorological stations collected between 1953 and 2022. This study focuses on analyzing regional snowstorm events. Winter is defined as the period from November to March of the following year. The climatological mean was calculated using the complete dataset spanning the period 1953-2022.

Objective classification method

The obliquely rotated principal component analysis (PCA) in T-mode (PCT) was applied to classify synoptic patterns, The selection of 500 hPa is because it can represent the evolution of synoptic systems in NX^{31,32}. The analysis utilized daily mean geopotential height fields derived from ERA5 reanalysis data. The PCT method performs better in terms of spatiotemporal stability of classification results compared to other methods³⁷. In the PCT model, the columns of the input matrix represent time observations, while the rows represent grid points. This method can capture the underlying physical structure while avoiding the emergence of large clusters, yielding more realistic and physically meaningful synoptic patterns. This method has now been integrated into the COST733Class software package. (https://cost733.met.no)^{38,39}. All figures are made by NCAR Command Language (Version 6.6.2), which is available at https://www.ncl.ucar.edu/.The software package of the objective classification method (COST733Class-1.2, Harmonization and Application of Weather Type Classifications for European Region) can be obtained from https://cost733.met.no/cost733/.

Moisture transport budget

To calculate the moisture budget under different synoptic patterns in the NX, the moisture flux (Q) was used to calculate the mass of moisture flowing through a unit area per unit of time. The calculation formula is as follows^{40,41}:

$$Q = -\frac{1}{g} \int_{P_{\circ}}^{p_t} V_n q dp \tag{1}$$

Where g is gravitational acceleration with units of m s⁻², q is specific humidity with units of kg kg⁻¹. In the calculation of vertically integrated water vapor flux, p_t denotes the pressure level at the top of integration (set to 300 hPa in this study), while P_s represents the bottom level, which uses the mean sea-level pressure value. The vertically integrated moisture flux was adopted as it provides a more complete characterization of thermodynamic processes. V_n denotes the component of wind velocity perpendicular to the plane through which the moisture flux is calculated with units of m s⁻¹. The unit of the Q is kg (m s)⁻¹, the calculation involves integrating from the surface to 300 hPa. In this study, AB, CD, EF, GH, IJ, KL, and MN are defined as the northern boundary, OP and QR as the southern boundary, RA, BC, DE, and FG as the western boundary, and HI, JK, LM, and NO as the eastern boundary (Fig. 2c-d). When calculating the values at each boundary, the following formulas were used:

$$Q_W = \sum_{i=1}^{m_1} Q_\alpha(i) \times d_W \tag{2}$$

$$Q_E = \sum_{i=1}^{m^2} -Q_\alpha(i) \times d_E \tag{3}$$

$$Q_S = \sum_{i=1}^{n_1} Q_{\beta}(i) \times d_S \tag{4}$$

$$Q_N = \sum_{i=1}^{n^2} -Q_{\beta}(i) \times d_N \tag{5}$$

$$Q_{SUM} = Q_W + Q_E + Q_N + Q_S \tag{6}$$

Where, Q_{α} and Q_{β} represent the zonal and meridional moisture fluxes. m1 and m2 represent the number of grid points on the western and eastern boundaries, while n1 and n2 represent the number of grid points on the southern and northern boundaries. The d_W and d_E represent the grid spacing of the western and eastern boundaries, while the d_S and d_N indicate the grid spacing of the southern and northern boundaries. Q_W , Q_E , and Q_N represent the moisture fluxes through the western, eastern, southern, and northern boundaries, respectively. And Q_{SUM} represents the net moisture flux. The positive directions are defined as eastward and northward, where i represents the grid point index. When the moisture flux across a given boundary is positive, it indicates moisture inflow, while a negative value denotes moisture outflow. The grid unit is meters (m).

Results Background

The terrain of NX is complex, with the Tianshan Mountains extending from the western to the eastern part of NX, and the Altai Mountains located to the northeast (Fig. 1). In the Ili and Tacheng, the unique topographic structure makes them high-frequency zones for extreme synoptic events^{11,42}. Over the past 70 years, the number of snowstorms in NX has shown an overall increasing trend (Figure S1). The 500 hPa climatological average circulation and wind field indicate that NX is primarily controlled by westerlies during the winter (Fig. 2b),

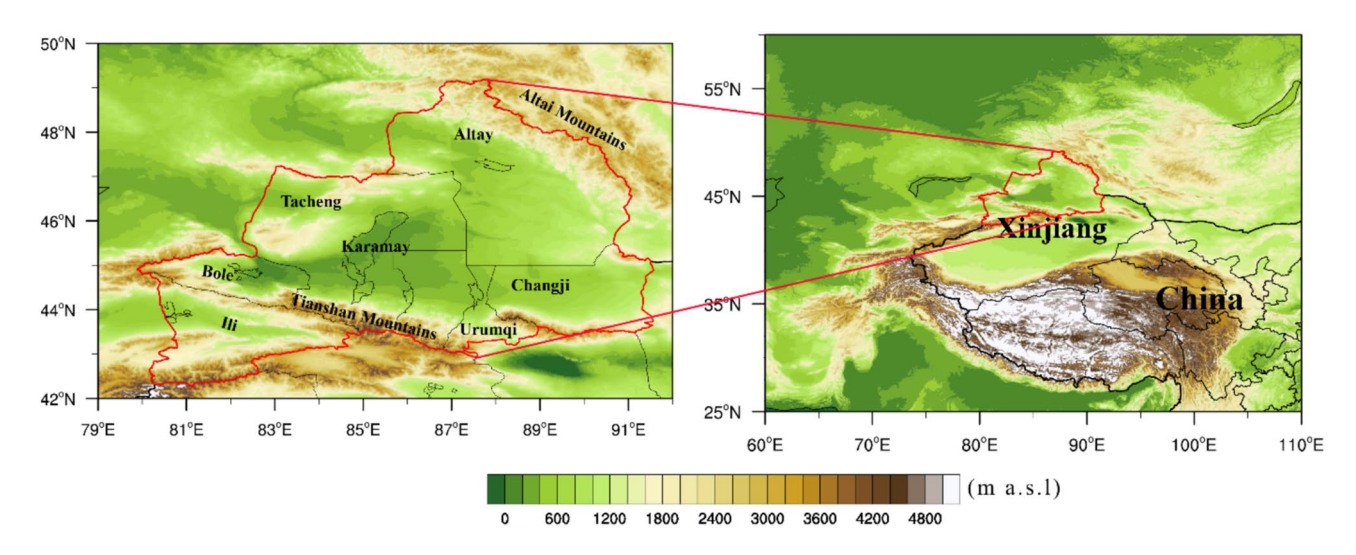


Fig. 1. Overview of the study area, with the red solid line representing the boundary of the NX, and the topography (shading, unit: m a.s.l).

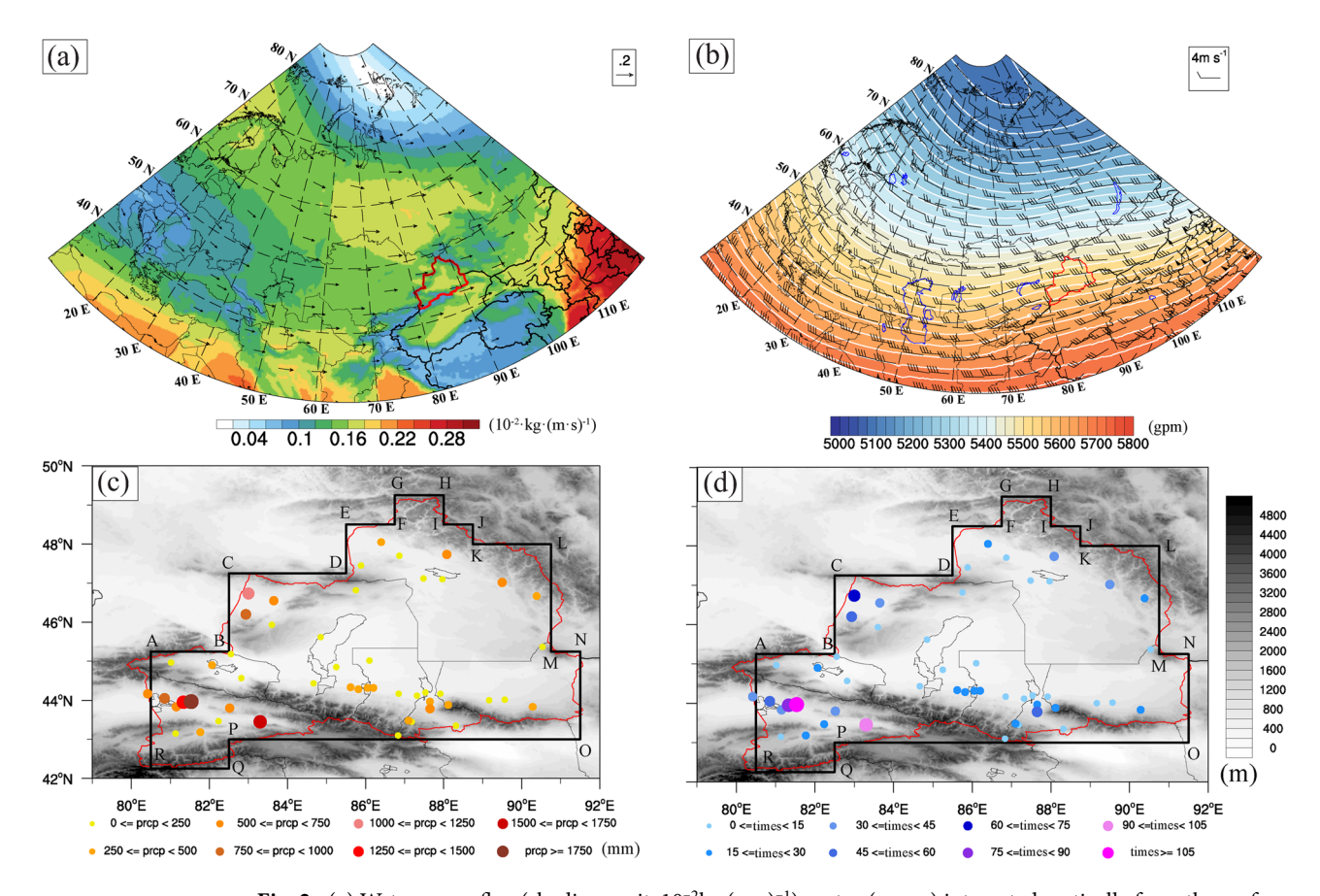


Fig. 2. (a) Water vapor flux (shading, unit: 10^{-2} kg (m s)⁻¹) vector (arrow) integrated vertically from the surface to the 300 hPa (b) Climatological mean of 500 hPa geopotential height (shading, unit: gpm) and wind field (wind barbs), with the blue solid lines represent lakes. (c) Total precipitation (unit: mm) reaching snowstorm levels at each station, along with topography (shading, unit: m). (d) Total number of snowstorm occurrences at each station. The horizontal and vertical thick straight lines in black in (c-d) indicate the boundaries for calculation of the meridional and zonal moisture flux. Each figure presents data for the winter seasons from 1953 to 2022.

with a polar vortex present in high-latitude regions and the low-pressure center located north of 80°N. At the same time, the climatological average vertically integrated (from the surface to 300 hPa) moisture flux shows that during winter, moisture is primarily transported from the western side to the NX, reaching 0.16 10^{-2} kg (m s)⁻¹ (Fig. 2a). The snowstorm distribution characteristics based on station data show that snowstorms primarily occur in Ili, Tacheng, Altay, and the northern slopes of the Tianshan Mountains (Fig. 2c–d). The accumulated snowstorm corresponds to the frequency of occurrence, which is consistent with the findings of Yang³¹. The maximum accumulated precipitation reaches 1894.9 mm, located in Ili, where the number of snowstorm occurrences is 113 (Fig. 2c–d). Another area of heavy precipitation is located in Tacheng, where the two stations on the western side experienced more than 45 snowstorms, with precipitation exceeding 750 mm. Snowstorms also occur frequently in other regions, such as the northern slopes of the Tianshan Mountains and areas along the Altai Mountains near Altay. More than 60 snowstorm events were recorded in Urumqi during 1953–2022.

Characteristics of snowstorms under typical synoptic patterns

The daily mean 500 hPa geopotential fields corresponding to the 134 days with regional snowstorm events in NX from 1953 to 2022 were classified using the PCT objective classification method. Figure 3 shows the classification results, dividing the 500 hPa geopotential height into four types (T1, T2, T3, and T4). The results indicate that T1 and T2 account for a larger proportion, reaching 82.8% of the total cases, while T3 and T4 types account for a smaller proportion, at 8.2% and 9%, respectively. The circulation patterns at the 700 hPa and 850 hPa levels are relatively similar for each type (Figures S2, S3).

In T1, there is a significant difference from the other three types. The polar vortex exhibits an eccentric pattern in high-latitude regions, with its low-pressure center located further south compared to the climatological average (Fig. 2b), and it extends towards northeastern Asia. The trough line extending from the polar vortex is located near Lake Balkhash, with NX situated in the front of the trough. T2 is similar to T3 and T4 because their polar vortices all exhibit a dipole structure, with one low-pressure center located over western Siberia and the other over Canada (not shown). The mid-to-high latitude regions show a meridional circulation pattern with one trough and one ridge, where the trough extends from northeastern Asia southward to the northwest of

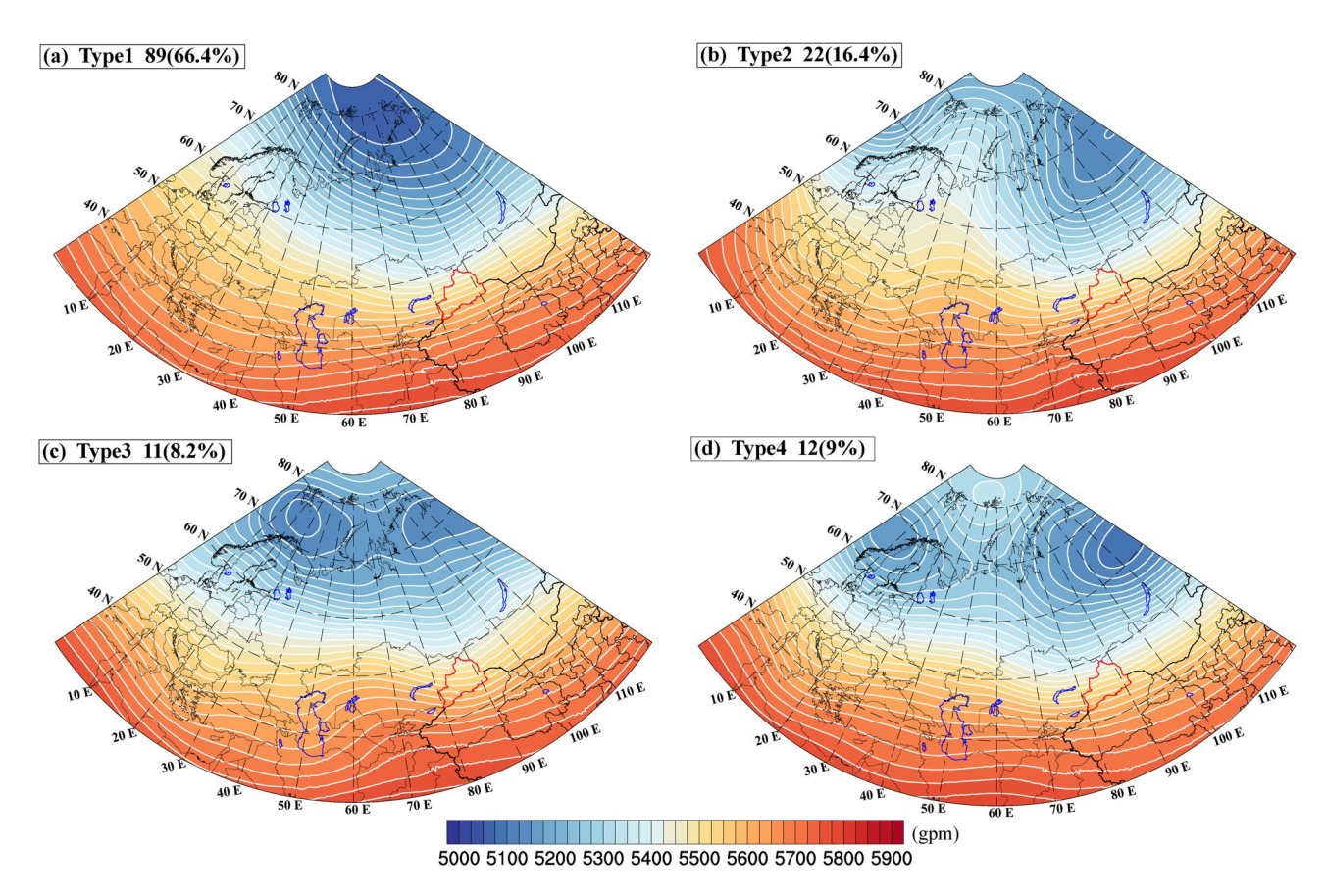


Fig. 3. (**a**–**d**) Mean daily distribution of the 500 hPa geopotential height for the period dominated by each synoptic type(shading, unit: gpm). The number and frequency of the cases in each pattern are shown in the upper left corner of each panel, with the red solid line representing the boundary of the NX, and the blue solid lines representing lakes.

NX, and the ridge is located over western Europe. Meanwhile, T3 and T4 both have two polar vortices, but the positions of the polar vortices differ. In T3, the polar vortices are close to each other (connected), whereas in T4, the configuration is more similar to T2, but the vortices are located closer to each other than in T2.

Figures 4 and 5 further examines the monthly distribution of snowstorms, precipitation intensity, total precipitation, and spatial distribution of snowstorm frequency under the four types. During the five winter months, T1 is the dominant type, except for January, when the numbers of T1 and T2 are comparable (Fig. 4a). Precipitation intensity in T4 is significantly higher than that in the other three types, while T1 and T3 have similar precipitation intensities, with T2 slightly higher (Fig. 4b). T4 exhibits the highest precipitation intensity, which is associated with its strongest low-level jet stream, concurrently accompanied by maximum moisture transport values in the lower troposphere. The spatial frequency of snowstorm occurrence for the four types is relatively similar in the Ili (Fig. 5), where the snowstorm frequency for T1 reaches over 50% at two stations. T1 and T2 show higher snowstorm occurrence frequencies in Tacheng. The precipitation distribution at each station that meets the snowstorm criteria shows that (Fig. 4c), except for T2, the other three types all exhibit extreme values exceeding 40 mm, with T4 reaching a maximum of 52.3 mm and an average of 18.0 mm, which is higher than the other types. For T3, the 25th and 75th percentiles, as well as the median and average values, are all lower than those of the other types. This is associated with its relatively weaker dynamic forcing and reduced moisture transport.

T3 differs significantly from the other types, as its high-frequency snowstorm zone is primarily concentrated along the northern slopes of the Tianshan Mountains, whereas the northern part of NX exhibits a lower frequency of occurrence. T3 also exhibits a high-frequency snowstorm area near Urumqi, which corresponds to the dynamic factors analyzed in the following Figs. 7 and 8.

As shown in Fig. 6a–d, among the four types, the NX is consistently located near the center of negative anomalies and is directly affected by them. T1 exhibits broader spatial influence from the interaction between its positive and negative anomaly centers compared to T2, although T2's positive anomaly center demonstrates greater intensity. In T1, the positive anomaly center over northern and eastern Europe couples with an elongated negative anomaly zone. For T2, its positive anomaly center over northern Russia is stronger than T1's, with a maximum climatology-extreme difference reaching 150 gpm, which relates to Rossby wave dynamics propagating to specific locations (Fig. 3b). T3 and T4 display more complex influencing factors due to multiple alternating positive or negative anomaly centers across mid-high latitudes. T3's positive anomaly center is closer

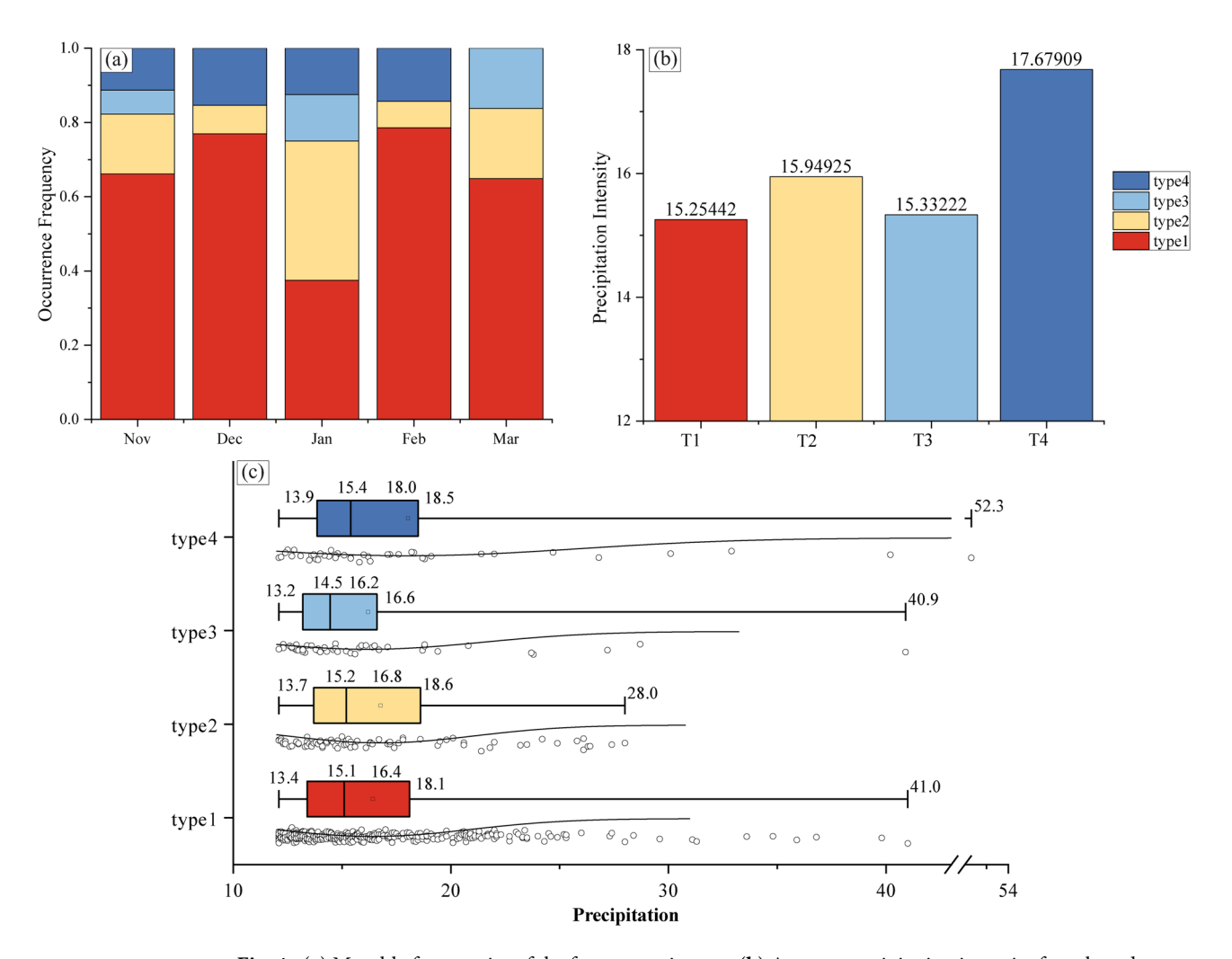


Fig. 4. (a) Monthly frequencies of the four synoptic types (b) Average precipitation intensity for selected synoptic types (unit: mm d^{-1}). (c) Distribution of precipitation amounts meeting the snowstorm criteria at each station under the four dominant synoptic types. The box in the box-and-whisker plot represents the 25–75th percentiles, containing both the mean and median values. The whiskers extend to the minimum and maximum data points, while the wavy line indicates the normal distribution.

to NX, situated near Lake Balkhash to the northwest of the region. The anomalous wind field indicates that T3 is characterized by strong anomalous northwesterly winds, with Fig. 3c revealing a pronounced northerly component in the westerly flow. This aligns with subsequent upper or lower-level jet stream analyses (Figs. 7 and 8). In contrast, T4's positive anomaly center resides over the Black Sea and regions north of 70°N. Notably, T4 demonstrates the strongest meridional moisture flux component at 850 hPa among all types (not shown).

Upper- and lower-level jets are often coupled and develop together⁴³. The lower-level jet is defined as regions with wind speeds of ≥ 12 m s⁻¹⁴⁴, while the upper-level jet is defined as regions with wind speeds of ≥ 30 m s⁻¹⁴⁵. The jet cores and their positions differ among the four types. The T1 upper-level jet stream covers most of the NX region with relatively weak intensity, and its jet core is located near Altay in eastern NX. T2 has the strongest jet intensity, with the jet core located over Tacheng. All identified synoptic types exhibit divergence zones on the right side of the upper-level jet stream axis, which aligns with fundamental characteristics of jet stream dynamics. At the same time, both T1 and T2 are associated with low-level jets at 700 hPa. The core of the lowlevel jet in T2 is located similarly to the upper-level jet core, with Tacheng located on the right side of the jet's exit region, accompanied by low-level convergence and upper-level divergence, which is favorable for the occurrence of heavy snow. T3 has weaker upper- and lower-level jet intensities compared to the other three types (Figs. 7c, 8c). The high frequency of snowstorms near Urumqi in T3 is associated with the jet stream's trajectory. The upper-level jet significantly influences Urumqi, accompanied by distinct upper-level divergence in this region-a feature that differs from other types (Fig. 7c). Meanwhile, due to its positive anomaly center being closer to the NX (Fig. 6c), the jet influences the western and southern parts of the NX from the northwest, with lower wind speeds near Altay. This is also related to the fewer snowstorms in the northern part of the NX in T3 (Fig. 5c). T4 has a weak upper-level jet stream, but the low-level jet stream is the strongest, which also leads to the strongest moisture transport in the middle and lower layers in T4 (Fig. 10d). For each type, the convergence region at

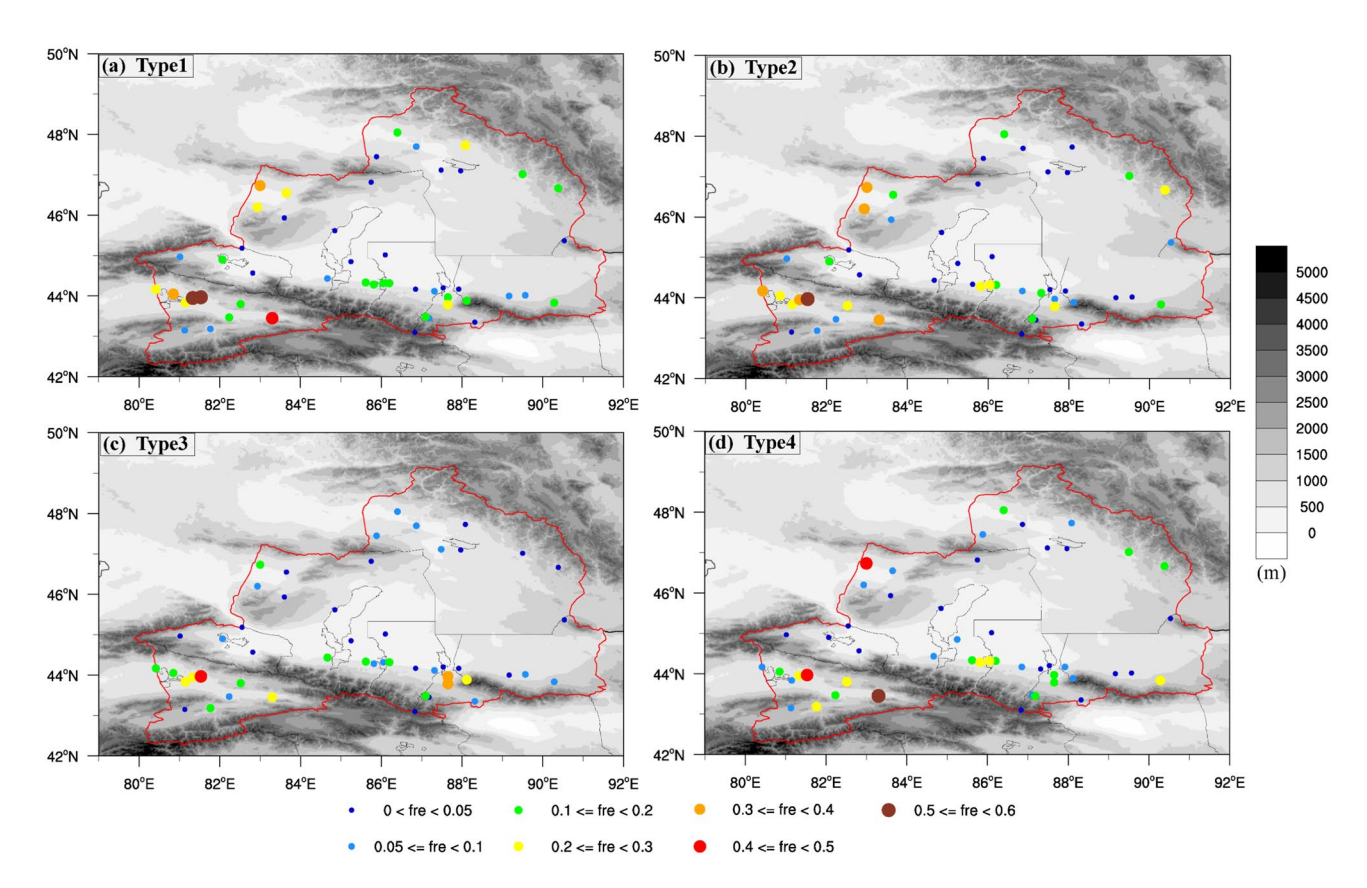


Fig. 5. (a–d) Frequencies of snowstorm occurrence at each station in NX under T1–T4. The red solid line represents the boundary of the NX.

lower levels corresponds to the divergence region at higher levels, which is conducive to generating vertical ascending motion.

Figures 9 show the integrated moisture flux from the surface to 300 hPa, with moisture primarily coming from the west. Moisture is transported into NX through three distinct pathways: one in Ili, one in Tacheng, and one in the northwest of Altay. Among these, the moisture flux intensity in T3 is weaker compared to the other three types, while T2 has the strongest flux. The integrated moisture flux across the entire layer reflects the overall moisture transport from the surface to higher altitudes. However, the moisture transport at different heights is not clearly defined, so we calculated moisture transport at different levels based on the four boundaries marked with black borders in Fig. 2c–d. The value for each direction is the sum of the values for all boundaries on the same side.

As shown in Fig. 10, moisture primarily enters from the west and exits to the east, with no significant differences observed among the four types. This indicates that the western side serves as the main boundary for moisture input for snowstorms. In terms of numerical values, moisture input from the west in T3 is noticeably lower than in the other types, and the same pattern is observed on the eastern side for moisture output. Additionally, in T3, moisture transport in the lower levels (surface to 700 hPa) is higher than in the mid-levels (700–500 hPa), which differs from the other types. On the northern side, all types except for T1 show moisture input, with the greatest difference (between T1 and T3) exceeding 90 times, The difference between T1 and T2 reached up to 40 times. At the same time, due to T4 having the strongest low-level jet (Fig. 8d), its mid- and lower-level moisture transport on the western side is stronger than that of the other three types.

Discussion

As noted earlier, snowstorm formation involves complex interactions among multiple factors, with atmospheric circulation and topographic forcing playing particularly critical roles. Previous studies have identified four high-frequency snowstorm zones in NX showing a significant increasing trend⁴⁶, which aligns with our findings. Synoptic analyses indicate that troughs and vortices are primary drivers of snowstorms in this region³¹. At the hemispheric scale, the winter polar vortex exhibits frequent southward displacements, predominantly adopting circumpolar and dipole configurations while lingering over the Northern Hemisphere⁴⁷. This study specifically examines the large-scale circulation patterns and dominant synoptic types associated with winter snowstorms in NX, with particular emphasis on the polar vortex's modulatory effects and pattern-dependent moisture transport mechanisms.

Recent work by Li et al. 13 employed observational data to subjectively classify snowstorm events based on snowfall distribution patterns, subsequently analyzing associated moisture transport and large-scale circulation

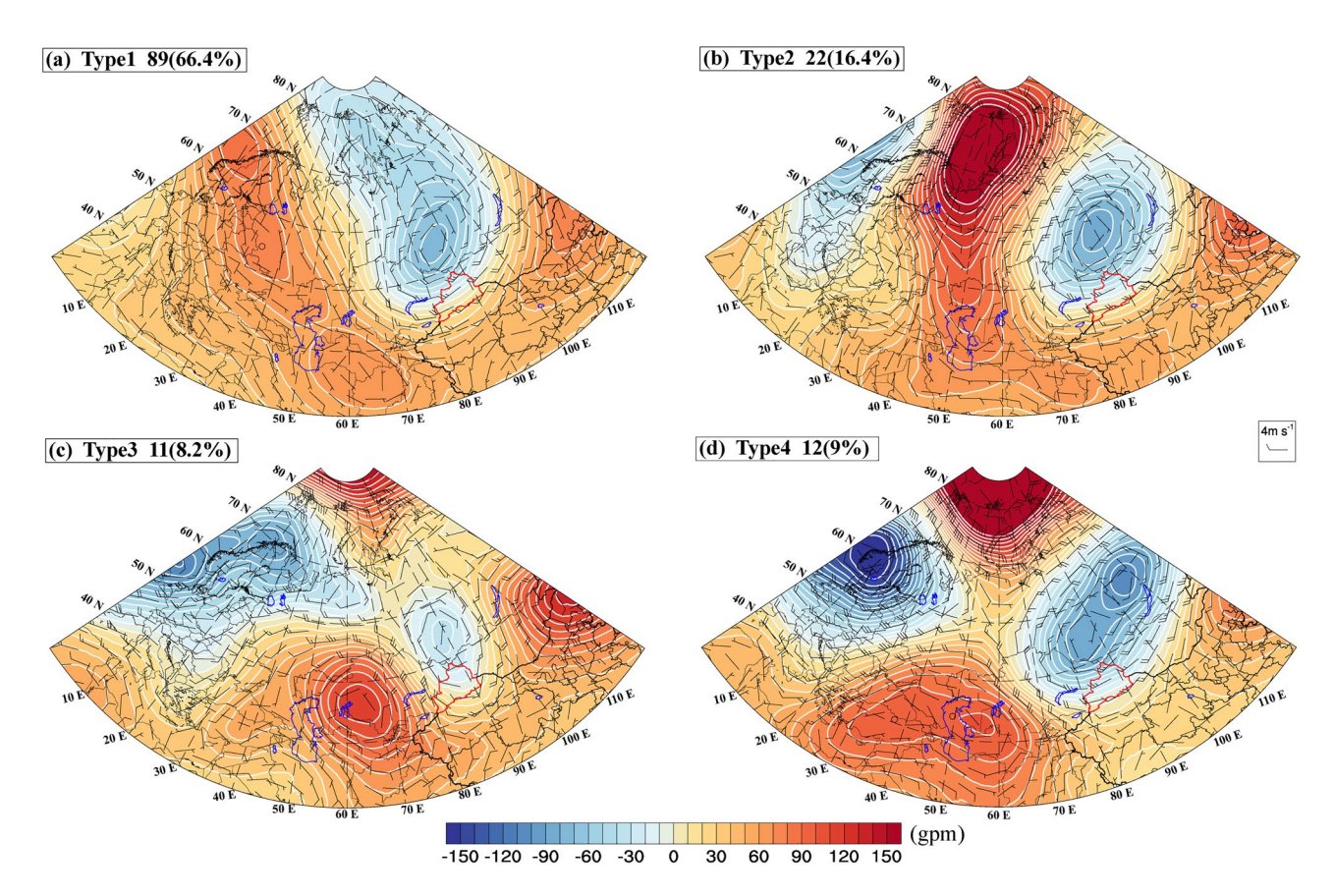


Fig. 6. (a–d) Anomaly of geopotential height (shading, unit: gpm) and wind field (wind direction bar) at 500 hPa under the four dominant synoptic patterns. The red solid line represents the boundary of the NX, and the blue solid lines represent lakes.

systems. However, their classification relied solely on spatial snowfall patterns, which may lead to inaccuracies due to the sparse station network across NX and the challenge of representing vast areas with limited point observations. To address this limitation, our study introduces an objective classification method for this region. By systematically categorizing large-scale circulation patterns, we identify distinct synoptic types influencing snowstorm events. Consistent with previous findings⁴⁷, our results confirm the crucial role of high-latitude polar vortex activity. All snowstorm events are associated with either eccentric or dipole vortices. Notably, while T2-T4 events all occur under dipole vortex conditions, their underlying mechanisms differ substantially. For instance, T2 exhibits the strongest upper-level jet but a relatively weak low-level jet, T4 shows the opposite vertical jet structure, and T3 demonstrates the most distinct characteristics among all types. These findings highlight that even under similar polar vortex regimes, detailed type-specific analysis remains essential for understanding snowstorm formation mechanisms.

Through analysis of upper- and lower-level jets for each synoptic type, we found they primarily enter the NX region from the west and northwest, which aligns with the conclusions of Wei et al.³³. However, that study did not examine the coupling between upper- and lower-level jets and their relationship with corresponding snowstorm occurrence areas. Our research emphasizes the specific jet stream configurations for each type and their connections with snowstorm spatial distributions and associated moisture transport characteristics. By conducting type-specific analyses of jet streams and moisture transport patterns under large-scale circulation backgrounds (based on objective classification), this study provides deeper insights into snowstorm mechanisms in this region. These findings will enhance snowstorm prediction accuracy under global warming trends.

In this objective classification study, the large sample size may lead to the neglect of non-representative features in comprehensive analyses, although these features are also important factors influencing snowstorm events in this region. Additionally, due to the limited temporal and spatial resolution of reanalysis data, fine-scale characteristics in many areas remain undetected. The sparseness of station data may also affect the completeness of the conclusions.

Conclusion

This study applies the PCT objective classification method to analyze 134 regional snowstorm events in NX during 1953–2022 using observational and reanalysis data, identifying four dominant synoptic patterns that account for 66.4% (T1) and 33.6% (T2–T4) of cases respectively. The results reveal that T1 features an eccentric polar vortex while T2–T4 exhibit dipole vortices with positional differences, with NX consistently located near

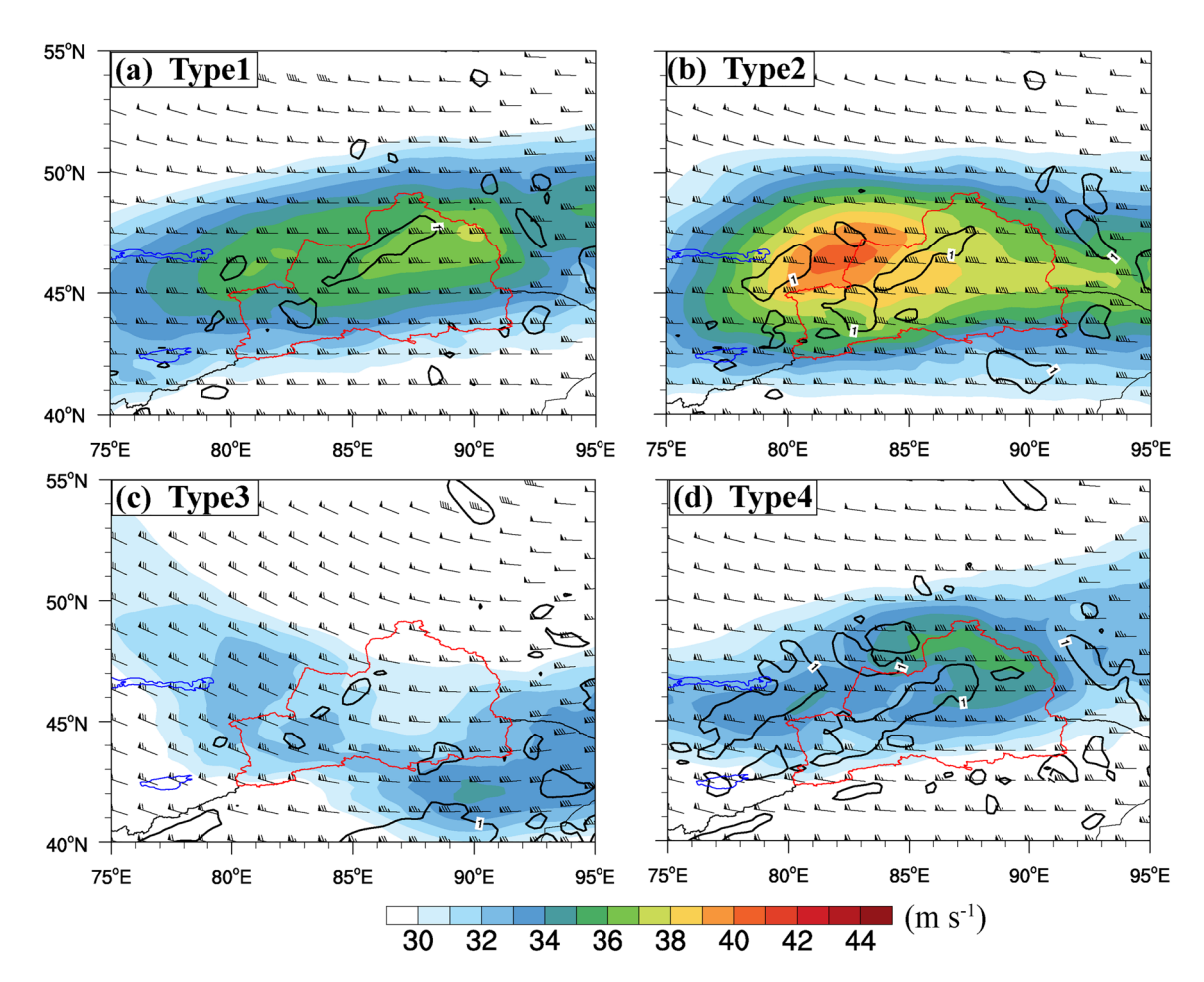


Fig. 7. (a-d) 300 hPa upper-level jet (unit: m s⁻¹), wind fields (wind direction bar), and the black solid line represents the area with divergence greater than 1×10^{-5} s⁻¹. The red solid line represents the boundary of the NX, and the blue solid lines represent lakes.

the 500 hPa negative anomaly center (stronger positive anomalies in T2). Particularly, T3 demonstrates distinct characteristics including marked northwesterly anomalous winds, jets with strong northerly components, and snowstorm concentration in western and southern regions, while variations in upper and lower-level jets directly affect snowstorm frequency and distribution. Moisture transport primarily occurs through western and northern boundaries (western dominant), with large-scale circulation causing significant differences in northern moisture input. Future research will employ detailed numerical simulations and sensitivity analyses to quantify topographic effects, thereby improving mechanistic understanding and prediction of snowstorm events.

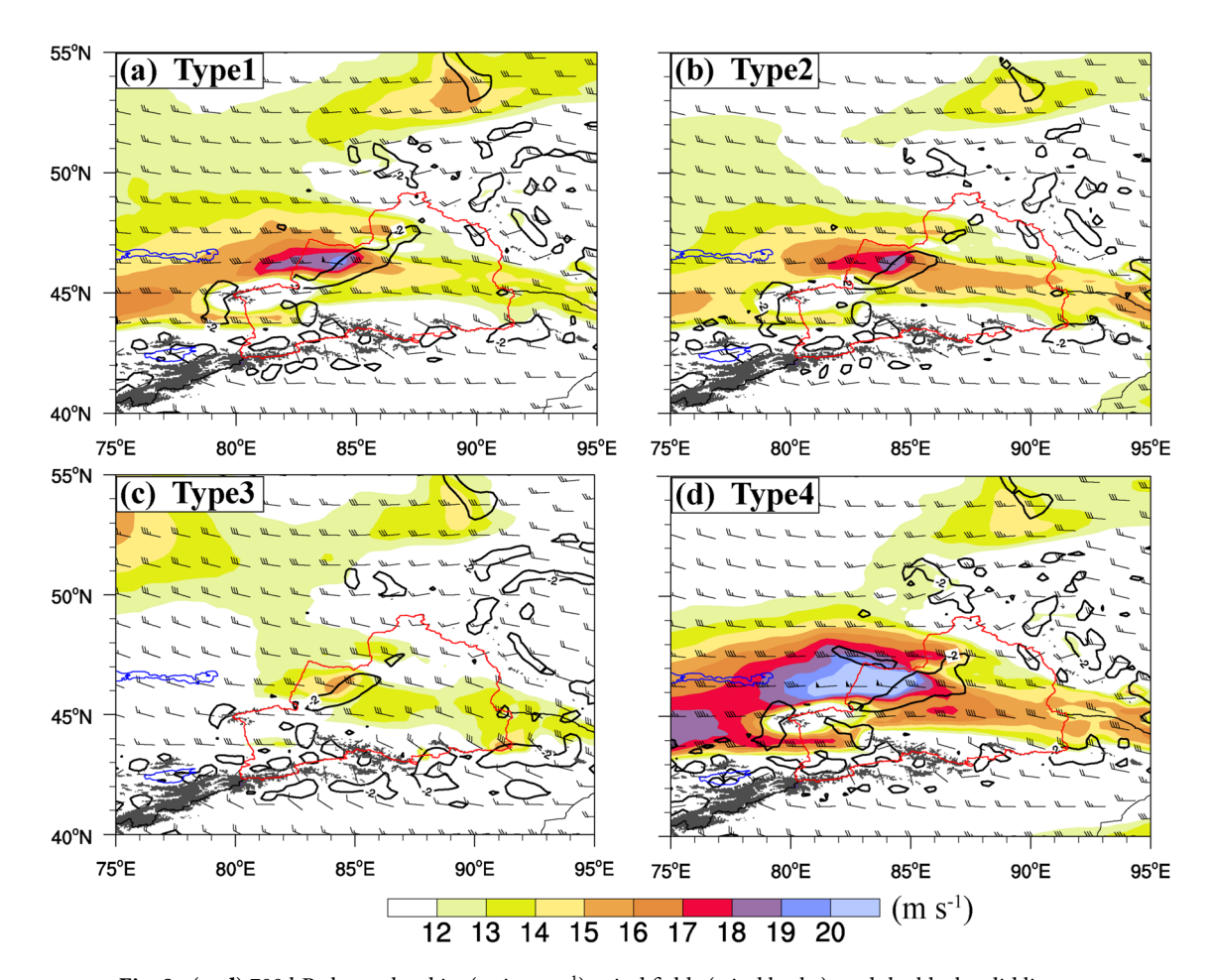


Fig. 8. (a–d) 700 hPa lower-level jet (unit: m s⁻¹), wind fields (wind barbs), and the black solid line represents the area with divergence less than -2×10^{-5} s⁻¹, and the topography (shading). The red solid line represents the boundary of the NX, and the blue solid lines represent lakes.

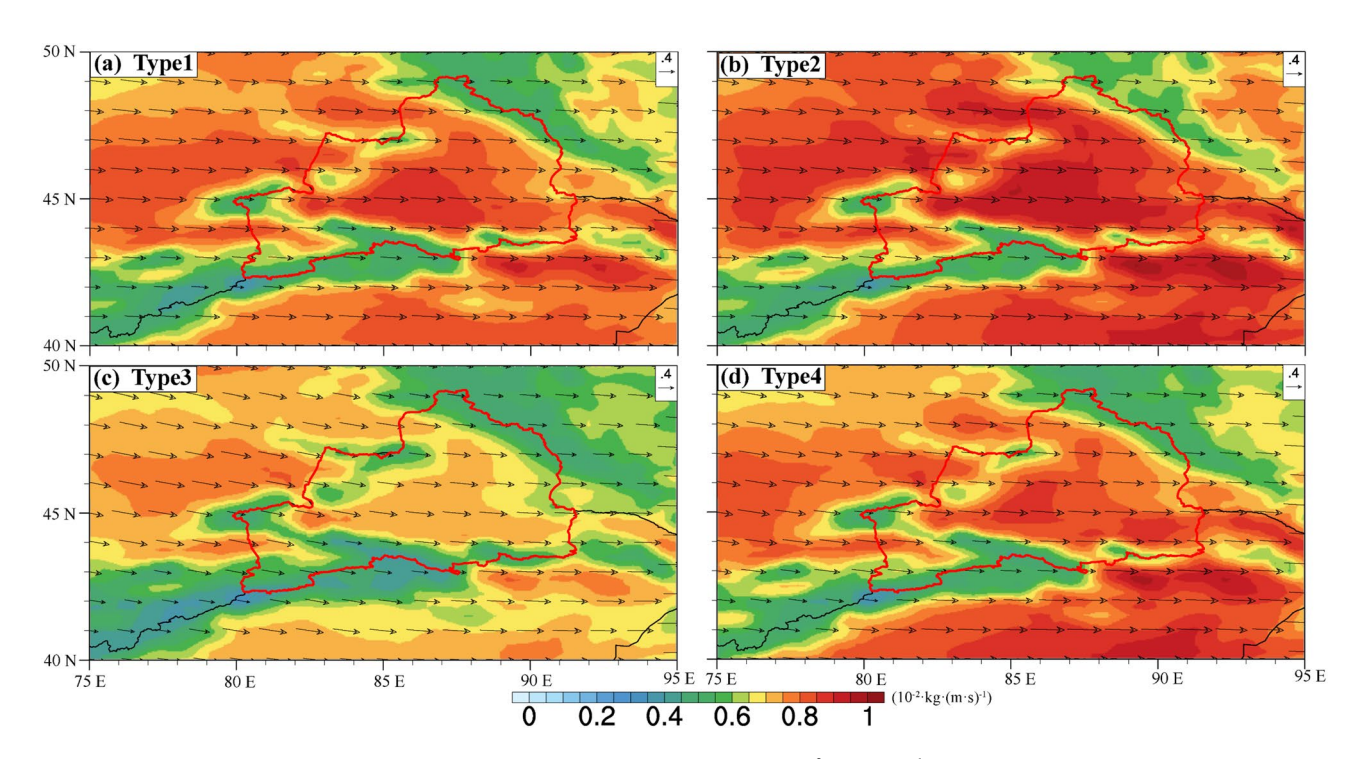


Fig. 9. (a–d) Moisture flux magnitude (shading, unit: 10^{-2} kg (m s)⁻¹) and vectors (arrows) integrated from the surface to 300 hPa for selected dominant synoptic patterns.

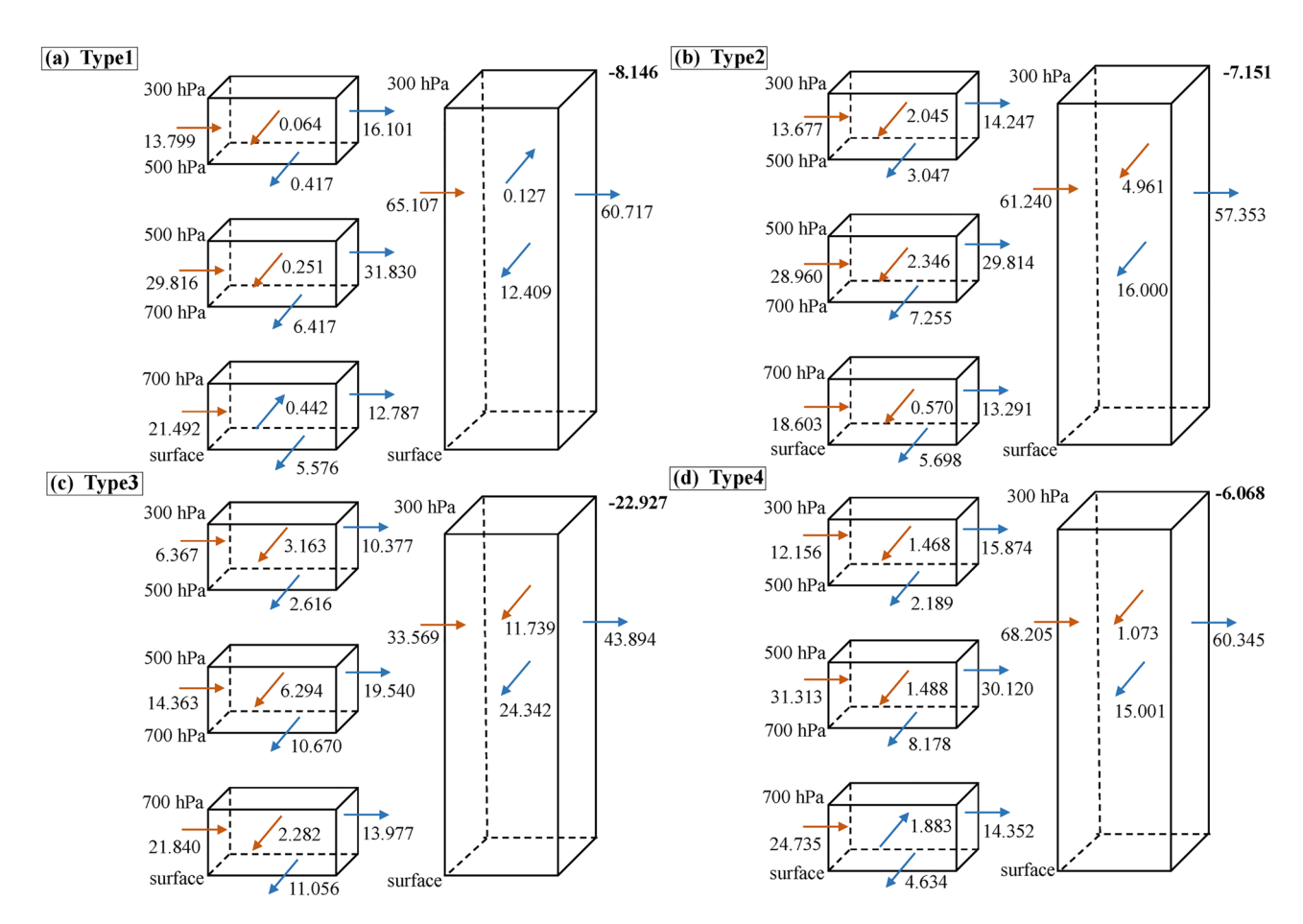


Fig. 10. (a–b) Vertical distribution of moisture flux at different levels (i.e., 300 hPa–500 hPa, 500 hPa–700 hPa, 700 hPa–surface) for the four types of patterns. Arrows represent the moisture flux magnitude (unit: 10^{-3} kg (m s)⁻¹) through the four boundaries of NX shown in the black boxes in Fig. 2c–d. Red arrows indicate inflow, blue arrows indicate outflow of moisture flux, and the numbers in bold larger fonts near the upper right corner of each box represent the net moisture flux at each level.

Data availability

The processed observational data employed in this research are available online (https://doi.org/https://doi.org/10.6084/m9.figshare.27276246). The ERA5 reanalysis data at pressure levels are available at https://cds.climate.copernicus.eu/datasets/reanalysis-era5-pressure-levels?tab=overview.

Received: 1 February 2025; Accepted: 9 June 2025 Published online: 01 July 2025

References

- 1. Burnett, A. W., Kirby, M. E., Mullins, H. T. & Patterson, W. P. Increasing Great Lake-effect snowfall during the twentieth century: A regional response to global warming?. *J. Clim.* 16, 3535–3542. https://doi.org/10.1175/1520-0442(2003)016%3c3535:Iglsdt%3e2 .0.Co;2 (2003).
- 2. Chen, Z. M. et al. Extreme rainfall and snowfall alter responses of soil respiration to nitrogen fertilization: A 3-year field experiment. *Glob. Change Biol.* 23, 3403–3417. https://doi.org/10.1111/gcb.13620 (2017).
- 3. Ue, M. A. O. et al. Microscale updrafts within northeast US coastal snowstorms using high-resolution cloud radar measurements. Mon. Weather Rev. 152, 865–889. https://doi.org/10.1175/mwr-d-23-0055.1 (2024).
- Bai, A., Zhai, P. M. & Liu, X. D. Climatology and trends of wet spells in China. Theoret. Appl. Climatol. 88, 139–148. https://doi.org/10.1007/s00704-006-0235-7 (2007).
- Donat, M. G., Lowry, A. L., Alexander, L. V., O'Gorman, P. A. & Maher, N. More extreme precipitation in the world's dry and wet regions. Nat. Climate Change 6, 508. https://doi.org/10.1038/nclimate2941 (2016).
- Chen, G. X., Wang, W. Y., Cheng, C. Z. E. & Hsu, H. H. Extreme snow events along the coast of the northeast United States:
 Potential changes due to global warming. J. Clim. 34, 2337–2353. https://doi.org/10.1175/jcli-d-20-0197.1 (2021).

 Moon S. et al. Anthropogonic warming induced intensification of summer moneous frontal precipitation every East. Acid. Sci. Adv.
- 7. Moon, S. et al. Anthropogenic warming induced intensification of summer monsoon frontal precipitation over East Asia. Sci. Adv. https://doi.org/10.1126/sciadv.adh4195 (2023).
- 8. Sun, J. Q., Wang, H. J., Yuan, W. & Chen, H. P. Spatial-temporal features of intense snowfall events in China and their possible change. *J. Geophys. Res. Atmos.* https://doi.org/10.1029/2009jd013541 (2010).
- Cao, Z. H., Xu, Q. & Zhang, D. L. Impact of cyclone-cyclone interaction on lake-effect snowbands: A false alarm. J. Geophys. Res. Atmos. https://doi.org/10.1029/2022jd037064 (2023).

- Colle, B. A. et al. An investigation of a Northeast US cyclone event without well-defined snow banding during IMPACTS. Mon. Weather Rev. 151, 2465–2484. https://doi.org/10.1175/mwr-d-22-0296.1 (2023).
- 11. He, X. et al. On the mechanisms of a snowstorm associated with a low-level cold front and low-level jet in the western mountainous region of the Junggar Basin, Xinjiang Northwest China. *Atmosphere* https://doi.org/10.3390/atmos14060919 (2023).
- 12. Zhai, L. et al. Characteristics of the mesoscale vortex in an extreme snowfall process in north China. *Meteorol. Monthly* 50(9), 1120–1128. https://doi.org/10.7519/j.issn.1000-0526.2024.071601 (2024).
- 13. Li, Y., Yang, L., Cheng, W. & Deng, Z. A diagnostic study of water vapor transport and budget during wintertime snowstorm days over different regions of northern Xinjiang during 1979–2017. *Chin. J. Atmos. Sci.* 48, 405–416. https://doi.org/10.3878/j.issn.100 6-9895.2204.21137 (2024).
- Veals, P. G., Steenburgh, W. J., Nakai, S. & Yamaguchi, S. Intrastorm variability of the inland and orographic enhancement of a seaeffect snowstorm in the hokuriku region of Japan. Mon. Weather Rev. 148, 2527–2548. https://doi.org/10.1175/mwr-d-19-0390.1
 (2020).
- 15. Gehring, J. et al. Orographic flow influence on precipitation during an atmospheric river event at davis Antarctica. *J. Geophys. Res.- Atmos.* https://doi.org/10.1029/2021jd035210 (2022).
- Suzuki, Y., Kawamura, R., Kawano, T. & Mochizuki, T. Cascading effects of the Changbai Mountains on an extreme weather disaster in northern Japan in January 2021. Weather Climate Extremes https://doi.org/10.1016/j.wace.2022.100439 (2022).
- 17. Chen, G. X. et al. Extreme snow events along the coast of the northeast United States: Analysis of observations and HiRAM simulations. *J. Clim.* 32, 7561–7574. https://doi.org/10.1175/jcli-d-18-0874.1 (2019).
- 18. Bergmaier, P. T. & Geerts, B. llap band structure and intense lake-effect snowfall downwind of lake Ontario: Insights from the OWLeS 7–9 January 2014 Event. J. Appl. Meteorol. Climatol. 59, 1691–1715. https://doi.org/10.1175/jamc-d-19-0288.1 (2020).
- 19. Huang, H., Tao, R., Zhao, K., Wen, L. & Chu, Z. Potential of snowfall nowcasting using polarimetric radar data and its link to ice microphysics: Study of two snowstorms in East China. *J. Geophys. Res. Atmos.* https://doi.org/10.1029/2022jd037654 (2023).
- 20. Melón-Nava, A. et al. Snowfall events in the Cantabrian Mountains of northwestern Spain: WRF multiphysics ensemble assessment based on ground and multi-satellite observations. *Atmos. Res.* https://doi.org/10.1016/j.atmosres.2023.106719 (2023).
- Sun, D. et al. Deep learning improves GFS wintertime precipitation forecast over southeastern China. Geophys. Res. Lett. https://doi.org/10.1029/2023gl104406 (2023).
- 22. Xu, X. K. et al. What are the dominant synoptic patterns leading to the summer regional hourly extreme precipitation events over central-eastern tibetan plateau and sichuan basin?. *Geophys. Res. Lett.* https://doi.org/10.1029/2022gl102342 (2023).
- 23. Utsumi, N., Kim, H., Kanae, S. & Oki, T. Which weather systems are projected to cause future changes in mean and extreme precipitation in CMIP5 simulations?. J. Gerontol. Ser. A Biol. Med. Sci. 121, 10522–10537. https://doi.org/10.1002/2016jd024939
- 24. Abulikemu, A. et al. Statistical characteristics of merger-type sea-breeze fronts and associated circulation patterns in the Bohai Bay region, North China. *Int. J. Appl. Earth Observ. Geoinform.* https://doi.org/10.1016/j.jag.2024.104005 (2024).
- Tang, Y. et al. Drivers of summer extreme precipitation events over east China. Geophys. Res. Lett. https://doi.org/10.1029/2021gl0 93670 (2021).
- 26. Wang, C., Chen, X., Zhao, K. & Peng, C.-H. Synoptic control on the initiation and rainfall characteristics of warm-season MCSs Over the South China coast. *J. Geophys. Res. Atmos.* https://doi.org/10.1029/2023jd039232 (2024).
- 27. Rao, X. et al. Influence of synoptic pattern and low-level wind speed on intensity and diurnal variations of orographic convection in summer Over Pearl River Delta, South China. *J. Gerontol. Ser. A Biol. Med. Sci.* 124, 6157–6179. https://doi.org/10.1029/2019jd 030384 (2019).
- 28. Li, M., Zhang, Q. & Zhang, F. Hail day frequency trends and associated atmospheric circulation patterns over China during 1960–2012. J. Clim. 29, 7027–7044. https://doi.org/10.1175/jcli-d-15-0500.1 (2016).
- 29. Wang, C., Zhao, K., Huang, A., Chen, X. & Rao, X. The crucial role of synoptic pattern in determining the spatial distribution and diurnal cycle of heavy rainfall over the South China Coast. J. Clim. 34, 2441–2458. https://doi.org/10.1175/jcli-d-20-0274.1 (2021).
- Zeng, J. W. et al. Typical synoptic patterns responsible for summer regional hourly extreme precipitation events over the middle and lower Yangtze River Basin China. Geophys. Res. Lett. https://doi.org/10.1029/2023gl104829 (2023).
- 31. Yang, X., Li, A., Zhao, Y. & Wei, J. Spatial-temporal distribution and general circulation of snowstorm in northern Xinjiang from 1961 to 2018. J. Glaciol. Geocryol. 42, 756–765. https://doi.org/10.7522/j.issn.1000-0240.2020.0060 (2020).
- 32. Li, A. et al. Circulation classification and cause analysis of the snowstorm case in Urumqi City from 1961 to 2019. *Arid Land Geograp.* 45, 379–388. https://doi.org/10.12118/j.issn.1000-6060.2021.214 (2022).
- 33. Wei, J., Wan, Y., Zhang, J., Zhao, F. & Li, A. Circulation classification and cause analysis of the warm-area blizzards in Tacheng area in recent 20 years. *Arid Land Geograp.* 45, 1718–1728. https://doi.org/10.12118/j.issn.1000-6060.2022.073 (2022).
- 34. Aran, M., Pena, J. C. & Torà, M. Atmospheric circulation patterns associated with hail events in Lleida (Catalonia). Atmos. Res. 100, 428–438. https://doi.org/10.1016/j.atmosres.2010.10.029 (2011).
- 35. Duolaite, X. Formulation of precipitation intensity standard of Xinjiang. *Bimonthly Xinjiang Meteorol.* https://doi.org/10.3969/j.issn.1002-0799.2005.03.003 (2005).
- 36. Yang, L. Xinjiang Baoxue Nianjian (1953-2017) (China Meteorological Press, 2018).
- 37. Huth, R. An intercomparison of computer-assisted circulation classification methods. *Int. J. Climatol.* 16, 893–922. https://doi.org/10.1002/(SICI)1097-0088(199608)16:8%3c893::AID-JOC51%3e3.0.CO;2-Q (1996).
- 38. Huth, R. et al. in *Trends and Directions in Climate Research* Vol. 1146 *Annals of the New York Academy of Sciences* (eds L. Gimeno, R. GarciaHerrera, & R. M. Trigo) 105–152 (2008).
- 39. Philipp, A., Beck, C., Huth, R. & Jacobeit, J. Development and comparison of circulation type classifications using the COST 733 dataset and software. *Int. J. Climatol.* 36, 2673–2691. https://doi.org/10.1002/joc.3920 (2016).
- Qu, L.-L., Yao, J.-Q. & Zhao, Y. Mechanism analysis of the summer dry-wet interdecadal transition in the Tarim Basin Northwest China. Atmospheric Res. https://doi.org/10.1016/j.atmosres.2023.106840 (2023).
- 41. Yao, J. Change in atmospheric and surface water resource in Xinjiang. Arid Zone Res. https://doi.org/10.13866/j.azr.2024.02.01 (2024).
- 42. Li, Z. et al. Diurnal variation characteristics of summer precipitation and related statistical analysis in the Ili Region, Xinjiang Northwest China. Remote Sensing https://doi.org/10.3390/rs15163954 (2023).
- 43. Uccellini, L. W. & Johnson, D. R. The coupling of upper and lower tropospheric jet streaks and implications for the development of severe convective storms. *Monthly Weather Rev.* https://doi.org/10.1175/1520-0493 (1979).
- 44. Lei, Y. The compositive analysis of the meridional type persistent severe rainstorms. *Acta Meteorol. Sinica* https://doi.org/10.1167 6/qxxb1981.019 (1981).
- 45. Duan, H., Yao, X., Liu, X., Zhou, G. & Zhao, C. Case study of the coupling mechanism of high- and low-level jets of the rainstorm process in west China. *Chin. J. Atmos. Sci. (in Chinese)* 47(6), 1907–1924. https://doi.org/10.3878/j.issn.1006-9895.2305.22120 (2023).
- 46. Yang, L. M., Jia, L. H. & Chang, T. Analyses of the climate characteristics and water vapor of heavy snow in Xinjiang Region. *J. Glaciol. Geocryol.* https://doi.org/10.7522/j.issn.1000-0240.2005.0058 (2005).
- 47. Li, J., Xu, H., Deng, J. & Ma, J. Long-term variability and causes of the tropospheric polar vortex over the northern hemisphere in winter. *Chin. J. Atmos. Sci.* 48, 2095–2109 (2024).

Acknowledgements

This work was sponsored by the National Natural Science Foundation of China (No. 42265003), Natural Science Foundation of Xinjiang Uygur Autonomous Region (No. 2022D01C359). We thank for the High-Performance Computing Center of Nanjing University for performing the numerical calculations in this paper on its IBM Blade cluster system.

Author contributions

Data curation: C.L.; formal analysis: C.L. and A.A. (Abuduwaili Abulikemu); investigation: C.L. and A.A. (Abuduwaili Abulikemu); methodology: A.A. (Abuduwaili Abulikemu); project administration: A.A. (Abuduwaili Abulikemu); resources: X.X., S.Z., A.A. (Abuduwaili Abulikemu); software: C.L., Z.L., M.M.,A.A. (Abidan Abuduaini) and Z.K. supervision: A.A. (Abuduwaili Abulikemu); validation: C.L., A.A. (Abuduwaili Abulikemu) and X.X.; writing-original draft: C.L., A.A. (Abuduwaili Abulikemu); writing-review and editing: C.L., A.A. (Abuduwaili Abulikemu). All authors have read and agreed to the published version of the manuscript.

Declarations

Competing interests

The authors declare no competing interests.

Additional information

Supplementary Information The online version contains supplementary material available at https://doi.org/10.1038/s41598-025-06474-z.

Correspondence and requests for materials should be addressed to A.A.

Reprints and permissions information is available at www.nature.com/reprints.

Publisher's note Springer Nature remains neutral with regard to jurisdictional claims in published maps and institutional affiliations.

Open Access This article is licensed under a Creative Commons Attribution-NonCommercial-NoDerivatives 4.0 International License, which permits any non-commercial use, sharing, distribution and reproduction in any medium or format, as long as you give appropriate credit to the original author(s) and the source, provide a link to the Creative Commons licence, and indicate if you modified the licensed material. You do not have permission under this licence to share adapted material derived from this article or parts of it. The images or other third party material in this article are included in the article's Creative Commons licence, unless indicated otherwise in a credit line to the material. If material is not included in the article's Creative Commons licence and your intended use is not permitted by statutory regulation or exceeds the permitted use, you will need to obtain permission directly from the copyright holder. To view a copy of this licence, visit http://creativecommons.org/licenses/by-nc-nd/4.0/.

© The Author(s) 2025